NeuroImage: Clinical 34 (2022) 103001

Contents lists available at ScienceDirect

NeuroImage: Clinical

journal homepage: www.elsevier.com/locate/ynicl

Patterns of white and gray structural abnormality associated with paediatric demyelinating disorders

Sonya Bells [a,b,c], Giulia Longoni [a,d,e], Tara Berenbaum [a], Cynthia B. de Medeiros [a], Sridar Narayanan [f], Brenda L. Banwell [g], Douglas L. Arnold [f], Donald J. Mabbott [a,h], E. Ann Yeh [a,d,e,*]

[a] Neurosciences and Mental Health Program, Research Institute, Hospital for Sick Children, Toronto, Canada
[b] Pediatric Neurology, Spectrum Health Helen Devos Children's Hospital, Grand Rapids, USA
[c] Department of Pediatrics and Human Development, Michigan State University, East Lansing, USA
[d] Department of Neurology, Hospital for Sick Children, Toronto, Canada
[e] Department of Paediatrics, University of Toronto, Toronto, Canada
[f] Department of Neurology and Neurosurgery, Montreal Neurological Institute and Hospital, McGill University, Montreal, Canada
[g] Division of Child Neurology, Children's Hospital of Philadelphia, Perelman School of Medicine, University of Pennsylvania, USA
[h] Department of Psychology, University of Toronto, Toronto, Canada

ARTICLE INFO

Keywords:
Multiple sclerosis
Myelin oligodendrocyte glycoprotein associated disorders
Diffusion
Optic neuritis
Fixel-based analysis
Cortical thickness

ABSTRACT

The impact of multiple sclerosis (MS) and myelin oligodendrocyte glycoprotein (MOG) - associated disorders (MOGAD) on brain structure in youth remains poorly understood. Reductions in cortical mantle thickness on structural MRI and abnormal diffusion-based white matter metrics (e.g., diffusion tensor parameters) have been well documented in MS but not in MOGAD. Characterizing structural abnormalities found in children with these disorders can help clarify the differences and similarities in their impact on neuroanatomy. Importantly, while MS and MOGAD affect the entire CNS, the visual pathway is of particular interest in both groups, as most patients have evidence for clinical or subclinical involvement of the anterior visual pathway. Thus, the visual pathway is of key interest in analyses of structural abnormalities in these disorders and may distinguish MOGAD from MS patients.

In this study we collected MRI data on 18 MS patients, 14 MOGAD patients and 26 age- and sex-matched typically developing children (TDC). Full-brain group differences in fixel diffusion measures (fibre-bundle populations) and cortical thickness measures were tested using age and sex as covariates. Visual pathway analysis was performed by extracting mean diffusion measures within lesion free optic radiations, cortical thickness within the visual cortex, and retinal nerve fibre layer (RNFL) and ganglion cell layer thickness measures from optical coherence tomography (OCT). Fixel based analysis (FBA) revealed MS patients have widespread abnormal white matter within the corticospinal tract, inferior longitudinal fasciculus, and optic radiations, while within MOGAD patients, non-lesional impact on white matter was found primarily in the right optic radiation. Cortical thickness measures were reduced predominately in the temporal and parietal lobes in MS patients and in frontal, cingulate and visual cortices in MOGAD patients. Additionally, our findings of associations between reduced RNFLT and axonal density in MOGAD and TORT in MS patients in the optic radiations imply widespread axonal and myelin damage in the visual pathway, respectively. Overall, our approach of combining FBA, cortical thickness and OCT measures has helped evaluate similarities and differences in brain structure in MS and MOGAD patients in comparison to TDC.

1. Introduction

Despite overlap between the clinical symptoms of multiple sclerosis (MS) and myelin oligodendrocyte glycoprotein (MOG)-associated disorders (MOGAD), recent phenotypical and pathological literature has established these entities to be distinct. The impact of paediatric-onset

* Corresponding author.
E-mail address: ann.yeh@sickkids.ca (E. Ann Yeh).

https://doi.org/10.1016/j.nicl.2022.103001
Received 6 December 2021; Received in revised form 21 March 2022; Accepted 30 March 2022
Available online 31 March 2022

MS and MOGAD on the structural integrity of the visual pathway is of particular interest, given the high likelihood of visual pathway involvement in both groups: most children with MS and MOGAD have evidence for either a clinical or subclinical event involving the optic nerve (Bennett et al., 2015; Ciftci-Kavaklioglu and Yeh, 2020; Eyre et al., 2018; Wilbur et al., 2019). Direct comparisons establishing similarities and differences of optic nerve damage on the rest of the brain and visual pathway in these disorders are greatly needed. Specifically, quantitative neuroimaging of both white- and grey- matter and retinal structural metrics from OCT, including retinal nerve fibre layer thickness (RNFLT) and ganglion-cell-inner-plexiform layer thickness (GCIPLT) may help to elucidate disease-specific patterns of structural abnormalities in the visual pathways of children with MS and MOGAD related disorders. Both disorders often affect the optic nerve, with discernable structural and functional abnormalities at the level of the retina (Ciftci-Kavaklioglu and Yeh, 2020). Identifying diagnosis-specific features on structural MRI may help further understand how MS and MOGAD differentially affect brain structure especially within the visual pathway.

Microstructural changes to white matter are often evaluated using diffusion tensor imaging (DTI) (Pierpaoli and Basser, 1996). DTI has been used extensively to study white matter abnormalities in children and adolescents with acquired demyelinating disorders within normal appearing white matter (NAWM), with a focus on global WM abnormalities in MS (Akbar et al., 2016; Aliotta et al., 2014; Aung et al., 2018; Klistorner et al., 2016; Kolasinski et al., 2012; Longoni et al., 2017; Pagani et al., 2005; Rocca et al., 2014a, 2014b; Till et al., 2011; Tillman et al., 2012; Vishwas et al., 2013, Vishwas et al., 2010). The widespread adoption of DTI relates to its high sensitivity to diffusional properties of white matter, clinically acceptable acquisition times and ease of modeling. However, it is limited in areas of complex microstructure, and provides a non-specific understanding of the biological abnormalities of brain development, such as demyelination, axonal loss, or oedema (Basser and Pierpaoli, 1996; Beaulieu, 2002; Beaulieu and Allen, 1994; Vos et al., 2012). Furthermore, most diffusion studies use voxel wise Tract-Based Spatial Statistics (TBSS; (Smith et al., 2006)), which attempts to improve on partial volume effects by projecting voxel data onto a 'skeleton'. However, this step ignores the rich directional information of diffusion imaging and is generally thought to be less biologically plausible (Raffelt et al., 2015). Higher-order diffusion models have allowed the development of analysis methods which are more sensitive to crossing fibres and boost specificity to white matter structure (Assaf and Basser, 2005; Dell'Acqua et al., 2013; Fieremans et al., 2011; Raffelt et al., 2012; Tournier et al., 2004; Tuch et al., 2003; Wedeen et al., 2005; Zhang et al., 2012).

Fixel-based analysis (FBA), one example of an advanced diffusion technique, can be used to quantify both microscopic and macroscopic changes to white matter fibres (Raffelt et al., 2015). Fixels are individually oriented fibre-bundle populations in a voxel. FBA is based on constrained spherical deconvolution (CSD), thus accounting for crossing fibres and is sensitive to structural intra-axonal volume changes (Raffelt et al., 2017). FBA includes three metrics: fibre density (FD), which reflects microstructural density of fibres/axons within a fibre bundle (Raffelt et al., 2012), fibre bundle cross section (FC), which assesses macrostructure and is sensitive to atrophy (Pannek et al., 2018), and a metric that combines both fibre density and fibre-bundle cross section (FDC), which is sensitive to both the density of axons and the area that the fibre bundles occupy (Raffelt et al., 2017). Abnormal white matter development is characterized by changes in FD, FC, and FDC. A decrease in FD suggests a decrease in intra-axonal volume fraction, meaning that the fraction of space occupied by the axons is smaller within a voxel. Smaller intra-axonal volume fractions may exist due to decreases in axonal diameter or axonal loss (i.e., less axons occupy this space). If a decrease in FD is measured while FC does not change it points to a change in intra-cellular volume, however if both decrease at the same time axonal loss can be indicated. FDC is reflective of WMs total capacity and can indicate how FD and FC influence WM change or injury. Fixel metrics are sensitive to axonal degeneration and loss and may offer greater pathologic specificity for axonal abnormalities than standard diffusion tensor metrics (Raffelt et al., 2017).

FBA enables the identification of white matter structure within a specific fibre bundle and has previously been used to investigate axonal density variation in normal development (Dimond et al., 2020). FBA metrics have demonstrated decreased FD and FDC (Gajamange et al., 2018) and FC (Storelli et al., 2020) related to diffuse white matter injury in adult MS. Additionally, alternative higher-order diffusion models such as neurite orientation and dispersion density imaging (NODDI), Composite Hindered and Restricted Model of Diffusion (CHARMED) (Santis et al., 2019), diffusion kurtosis imaging (DKI) (Chuhutin et al., 2020; Kelm et al., 2016), and DKI combined with biophysical models (Chuhutin et al., 2020) are useful to measure differences in white matter microstructure between demyelinating disorders and healthy populations (Granberg et al., 2017; Hagiwara et al., 2019). The white matter tract integrity (WMTI) model, an extension of the DKI model, evaluates white matter microstructure through quantification of axonal water fraction (AWF) and tortuosity of the extra-axonal space (TORT) (Fieremans et al., 2011; Veraart et al., 2013). This may be of use in paediatric MS and MOGAD patients, as previous adult studies have detected axonal injury along the posterior visual pathway (optic radiations) in MS patients (Gajamange et al., 2018; Hagiwara et al., 2019). Collectively, FBA and WMTI diffusion models may improve the specificity for microstructural changes, such as the ability to differentiate between abnormal axons and myelination, within the optic radiation in paediatric MS and MOGAD patients.

Finally, injury to grey matter, particularly cortical thinning, is well characterized in adults with MS (De Meo et al., 2019; De Stefano et al., 2014; Geurts and Barkhof, 2008; Steenwijk et al., 2016; Tsagkas et al., 2020). Cortical thickness, the distance between the white and grey matter surfaces (Dahnke et al., 2013), provides information on neural loss or degradation (Dahnke et al., 2013; Yotter et al., 2011) in MS (Popescu et al., 2015). Furthermore, grey matter atrophy or cortical thinning, a central feature of MS (Filippi et al., 2014; Geurts et al., 2012), presents at an early stage of the disease (Bergsland et al., 2012; Calabrese et al., 2007). Cortical thinning has been demonstrated in adults with MS within the frontal and temporal lobes (Sailer et al., 2003; Steenwijk et al., 2016) and posterior cingulate cortex (Steenwijk et al., 2016), which has been confirmed using histology (Peterson et al., 2001; Popescu et al., 2015). Studies that have measured cortical thinning within the paediatric MS population have focused on visual regions (Datta et al., 2019; Waldman et al., 2020) or mean whole brain changes (De Meo et al., 2021), and there are no studies evaluating cortical thickness in the paediatric MOGAD population.

The aim of this study was to examine the structure of white matter pathways and cortical thickness in children and adolescents with MS versus MOGAD including: (a) the whole brain and (b) within visual pathway structures. We performed a cross-sectional study, comparing paediatric patients diagnosed with MS or MOGAD to typically developing children (TDC). Specifically, we conducted whole brain FBA and cortical thickness analyses, and further performed targeted analyses of abnormalities in white and grey matter structures of the visual pathway and in structural OCT evaluations of the RNFLT and GCIPLT. To perform the targeted analyses while covarying for number of ON episodes, we extracted optic radiation regions that were lesion-free to investigate abnormal white matter using FBA metrics and voxel based WMTI metrics - AWF and TORT. We hypothesized widespread abnormalities in both MOGAD, and MS patients compared to healthy youth, but based on previous research greater differences within white and grey matter in the visual pathway in MOGAD relative to MS. We hypothesize that the axonal damage, as assessed by FBA and WMTI metrics, is present in MS and MOGAD patients and is associated with visual cortex thinning. We also hypothesized that insult to the anterior visual system – RNFLT and GCIPLT measured by optical coherence tomography (OCT) – would be related to WM changes along the posterior visual pathway – optic

radiation.

2. Materials and methods

2.1. Participants

We recruited children and adolescents presenting to the Neuroinflammatory Disorders program at the Hospital for Sick Children (SickKids) in Toronto with recurrent demyelinating syndromes. We defined MS following the Revised 2017 McDonald criteria (Thompson et al., 2018). MOGAD related disorders were identified by serum testing performed in a commercial laboratory using live, cell-based methods (Oxford, UK) (Kitley et al., 2014). We defined MOGAD positivity as having one positive test from a cell-based assay with 30 days (median 43.5 days 12.7 IQR) of their initial inflammatory event. Individuals with persistently positive MOGAD titres were also identified by serial measures at baseline and in follow up at a minimum of 6 months after onset (median 1.2 years 0.6 IQR) (Kitley et al., 2014). A comparison cohort of age matched TDC and adolescents were also recruited through advertisements. Institutional Research Ethics Board approval and written informed consent (or assent and informed consent from a parent/legal guardian depending on child's capacity to consent) from each participant was obtained prior to study initiation. All eligible participants were: (i) between 5 and 18.9 years of age, and (ii) spoke English as their native language or has had at least two years of schooling in English. Additional inclusion criteria for patients were (1) presence of an acute neuroinflammatory event (diagnosis of either MOGAD or MS) and (2) assessment at greater than 3 months since onset of symptoms or relapse. Excluded participants had a history of: (i) other neurological conditions, (ii) major medical comorbidities, (iii) major psychiatric comorbidity, (iv) learning disability, (v) traumatic brain injury, (vi) alcohol or illicit drug abuse, or (vii) non-demyelinating aetiologies of white matter dysfunction (i.e., metabolic disorders, vasculitis, and non-specific MRI abnormalities), (viii) cerebral palsy, and (ix) patients with <30 days since last steroid treatment. Additional exclusion criteria included (1) the need for sedation during imaging and (2) history of claustrophobia.

Optic neuritis events were defined as inflammatory episodes of decreased visual acuity lasting longer than 24 h and associated with either prolonged p100 on Visual Evoked Potential testing (using electroencephalogram), increased retinal nerve fibre layer (RNFL) thickness (RNFLT) on OCT (a surrogate for optic swelling), or MRI evidence of inflammation in the corresponding optic nerve. **Relapses** were defined as neurological events lasting longer than 24 h presumed to be inflammatory in origin accompanied by objective neurological findings and/or MRI abnormalities consistent with inflammation and corresponding to the neurological findings.

2.2. Imaging data

All participants were scanned on a 3T Siemens Prisma system (Siemens Medical Solutions, Erlangen, Germany) at SickKids in Toronto. We acquired the following MRI sequences: (i) an axial turbo spin-echo proton density [1x1x3mm; repetition time (TR) = 2200ms; echo time (TE) = 10ms; turbo factor 4]; (ii) an axial T2-weighted turbo spin-echo [1x1x3mm; TR = 4500ms; TE = 84ms; turbo factor 11]; (iii) an axial T1-weighted, 3D magnetization prepared rapid gradient echo (MPRAGE) sequence [0.9x0.9x1.0mm; TR = 1910ms; TE = 3.51ms; flip angle = 9 deg, TI = 1100ms]; (iv) a sagittal 3D FLAIR sequence [1x1x1mm; TR = 6000ms; TE = 356ms; TI = 2200ms] and (v) three sets of diffusion-weighted images using a single shot spin echo-sequence with an echo planar imaging readout [TR = 3800ms; TE = 73.0ms; FOV = 244x244mm, 70 slices, slice thickness = 2.0mm, no gap, bandwidth = 1952 Hz/pixel, 2 × phase encoding polarities (anterior-posterior) along 35, 45 and 66 directions for b-values of 1000, 1600 and 2600s/mm^2]. Participants had the option to watch a movie of their choice through video goggles to prevent excessive head movement during the scan.

2.3. Data and Code availability statement

In accordance with terms of consent given by participants or legal guardians, raw data utilized in this study are not available for sharing. Even so, processed data (mean values within regions of interest) are available upon request. Code utilized for data analysis are publicly available and provided on the software packages' websites (URLs provided in text when applicable). This policy is in accordance with the Research Ethics Board at the SickKids in Toronto.

2.4. OCT data

Each participant had spectral domain OCT conducted on the same day as the MRI using an OCT scanner (Carl Zeiss Meditac) by a trained technician. Serial optic disc and macula 200x200 cube scans were recorded with good centration, quantifying a 6x6x2mm volume. OCT scan quality scores of greater than 7 were considered acceptable and with no overt movements as detected by observing blood vessel discontinuity in the OCT face image. RNFLT and GCIPLT were assessed by quadrants and by average thickness; the average of all anatomic quadrants is reported for average RNFLT (μm) and GCIPLT (μm).

2.5. Imaging data Pre-processing

2.5.1. Tissue segmentation and lesion masks

For participants with demyelinating syndromes (MS or MOGAD), lesions were segmented at the McConnell Brain Imaging Centre, The Neuro (Montreal, QC, Canada) using an automatic change detection naïve Bayesian algorithm that classifies tissue using changes within T1, T2, proton density-weighted and FLAIR images (Elliott, 2016). After automatic lesion segmentation, lesions were then reviewed and manually corrected, if necessary, by trained personnel with expertise in demyelinating lesion identification. T1-weighted images were also used to segment tissue (white and grey matter) using a random forest classifier within the brain tissue segmentation pipeline (BISON), which is part of the MNI tools (https://bic-mni.github.io/). The T1-weighted images for each participant were registered to their corresponding diffusion space with a 12-parameter affine transformation using Advanced Normalization Tools (ANTs) (Avants et al., 2014). We would like to note that lesions within MOGAD tend to resolve over time in many cases. However, the majority of our MOGAD patients had brain lesions during our study and therefore felt that the total lesion volume could be of utility in these children.

2.5.2. Diffusion-weighted MRI pre-processing

Diffusion-weighted images were processed using the DESIGNER pipeline (Ades-Aron et al., 2018) (https://github.com/NYU-DiffusionMRI/DESIGNER or https://hub.docker.com/r/dmri/neurodock). Diffusion-weighted pre-processing steps included: denoising using Marchenko-Pastur principal component analysis technique (Veraart et al., 2016b, Veraart et al., 2016a), Rician bias correction within MRtrix (Version 3.0 rc2; https://mrtrix.readthedocs.io/en/latest/index.html) (Tournier et al., 2019), Gibbs' ringing correction (Kellner et al., 2016), EPI distortion correction using *topup* (Andersson et al., 2003) in FMRIB's Software Library (FSL) version 5.0.11, eddy current and motion correction using *eddy* in FSL (Version 5.0.11) (Andersson and Sotiropoulos, 2016), and signal outlier detection (Collier et al., 2015).

2.5.3. FBA of diffusion-weighted data

The following FBA steps were processed within MRtrix (Version 3.0.2) (Tournier et al., 2019). Response functions for white matter, grey matter and cerebrospinal fluid were generated for each participant using a fully automated unsupervised algorithm that has been successfully used with lesion data (Dhollander et al., 2019, 2017, 2016; Mito et al., 2018a, Mito et al., 2018b). A group averaged response function for each tissue type was created using TDC; patients were left out due to their

pathology. All DWIs and masks were upsampled to $1.3mm^3$ prior to fibre orientation distribution (FOD) estimation using multi-shell multi-tissue constrained spherical deconvolution (MSMT-CSD; (Jeurissen et al., 2014)). To achieve FOD amplitude correspondence between participants, global intensity normalisation was performed within MRTrix and applied to all participants' white matter FODs. A FOD template was created from 30 participants (15 TDC and 15 patients with the smallest lesion load (8MS and 7 MOGAD)) (Raffelt et al., 2012, Raffelt et al., 2011). All participants' FOD images and brain masks were non-linearly registered to the FOD template (Raffelt et al., 2012, Raffelt et al., 2011). The apparent fibre density (AFD) metric is estimated from the FOD template, which identifies the number and orientation of fixels in each voxel (Smith et al., 2013). Subsequently, fixel-based metrics FD, FC and FDC were calculated (Raffelt et al., 2017).

Next, whole-brain probabilistic fibre tractography on the FOD template was performed (20 million streamlines, termination cut-off 0.6, angle 22.5, max length 250mm, min length 10mm) using the iFOD2 algorithm (Tournier et al., 2010). The tractogram was then filtered to reduce the number of streamlines to 2 million using spherical-deconvolution informed filtering of tractograms algorithm (SIFT2; (Smith et al., 2013)) to reduce global reconstruction biases. Prior to statistical analysis, a fixel-fixel connectivity matrix was computed and fixel metrics were smoothed.

2.5.4. WMTI analysis of diffusion-weighted data

The following steps were processed using the tool from https://github.com/NYU- DiffusionMRI/Diffusion-Kurtosis-Imaging. The WMTI model consists of two microstructural environments (intracellular and extracellular) and its parameters are calculated using weighted linear least squares from the multi-shell pre-processed diffusion data (Ades-Aron et al., 2018; Fieremans et al., 2011). Subsequently, the following WMTI metrics were calculated (Fieremans et al., 2011; Veraart et al., 2013):

i. AWF is the ratio of water in the intra-axonal space to the total amount of water in a voxel, where decreases are presumed to represent axonal loss.
ii. TORT is the ratio of axial extra-axonal diffusivity to the perpendicular extra-axonal diffusivity, which is presumed to be a marker of myelin content.

Each participant's metric map of AWF and TORT was transformed to the population template space applying the FOD-drive transformations used in the previous FBA section.

2.5.5. Cortical thickness processing

Structural T1-weighted images were processed and analysed using the Computational Anatomy Toolbox (CAT12) (Gaser, C. Structural Brain Mapping, Group, Jena University Hospital, Jena, Germany; https://www.neuro.uni-jena.de/cat/) implemented in Statistical Parametric Mapping (SPM12; Wellcome Trust Centre for Neuroimaging, London, UK; https://www.fil.ion.ucl.ac.uk/spm/software/ spm12/). Processing and analysis steps were followed according to the pre-set parameters with the standard protocol described in the manual (https://www.neuro.uni-jena.de/cat12/CAT12-Manual.pdf). These steps included a statistical quality control step for inter-subject homogeneity and overall image quality of the T1-weighted images. Total intracranial volume (TIV) was calculated for use as a covariate in FBA statistical analysis to account for relative differences in head size which may vary during development. A mesh of the central surface (surface between the boundaries of grey matter/cerebro spinal fluid (CSF) and white/grey matter) was created using a projection-based distance method allowing for cortical thickness estimates (Dahnke et al., 2013). Cortical thickness estimations were resampled and smoothed using a 15mm full-width-half-maximum Gaussian kernel prior to group analysis.

2.6. Statistical analysis

2.6.1. Demographics

Independent Kruskal-Wallis tests were utilized to compare age, total intracranial volume (TIV), time since diagnosis, age of disease onset, Expanded Disability Status Scale (EDSS), RNFLT, GCIPLT and lesion volume between groups, while chi-squared tests were utilized to compare sex, number of clinical events, optic neuritis (ON) episodes, time between last ON episode and OCT acquisition. If the Kruskal-Wallis test was deemed to be significant a post-hoc pairwise multiple comparison Dunn Test adjusted with the Bonferroni method was performed to determine which groups are different. Analysis was conducted in R version 4.0.2 (R Core Team, 2020).

2.6.2. Whole brain FBA

Whole brain tractogram statistical analyses on fixel images, in study specific template space, were done using an intrinsic normalisation of the connectivity-based fixel enhanced (CFE) method (Raffelt et al., 2015; Smith et al., 2019) within MRtrix. The advantage of this method is that it considers crossing fibres, using tractography, and it includes information along white matter pathways during its statistical inference estimation. Group differences in fixel metrics (FD, FC and FDC) between TDC and patients were estimated at each white matter fixel using a General Linear Model (GLM) with age, sex and TIV as nuisance covariates. Statistical significance using an intrinsic normalisation was assessed using 5000 permutations and family-wise error (FWE) corrected $p < 0.05$ (Nichols and Holmes, 2002).

2.6.3. Cortical thickness

Surface-based statistical analysis was performed within CAT12/SPM12 (Gaser, C. Structural Brain Mapping, Group, Jena University Hospital, Jena, Germany; https://www.neuro.uni-jena.de/tfce; Wellcome Trust Centre for Neuroimaging, London, UK; http:// https://www.fil.ion.ucl.ac. uk/spm/software/spm12/). Group differences within cortical thickness measures were estimated using analysis of variance (ANOVA) with age and sex as nuisance covariates. We tested group differences using a threshold of $p < 0.05$ with FWE correction for multiple comparisons. Further, if a significant group effect was found, post-hoc pairwise t-tests were computed to detect differences between groups (threshold-free cluster enhancement (TFCE) correction for multiple comparisons) (Smith and Nichols, 2009).

2.6.4. Region of Interest analyses of white matter metrics within the optic radiations

We performed further region of interest analyses focused on the optic radiations bilaterally. The Johns Hopkins University (JHU) DTI-based white matter atlas (ICGM-DTI-81) (Mori et al., 2008) was non-linearly registered to each participant's diffusion space and then transformed to FOD template space to extract bilateral optic radiation regions of interest. Lesion masks for each patient were subtracted from their optic radiation region of interest to ensure only normal appearing white matter was analysed. Mean FD, FC, FDC, AWF and TORT were calculated within each optic radiation and independent Kruskal-Wallis tests were utilized to compare means between groups (R version 4.0.2 (R Core Team, 2020)).

3. Prediction of white matter metrics in the optic radiations using cortical and OCT thickness metrics

Linear mixed effects modelling fit by restricted maximum likelihood was used to assess whether cortical thickness in the primary visual cortex (V1) and OCT measures (RNFLT and GCIPLT) predict white matter metrics (FD, FC, FDC, AWF and TORT) in the optic radiations. Separate models were run for each patient group based on presumed visual pathway differences. The linear mixed effects models were generated using lmer function in R (lm4; (Bates et al., 2014)) in

conjunction with the package *sandwich* and *jtools* for robust standard errors (HC3) and *p*-values were generated. Sex, age, and time since diagnosis were set as fixed factors and participant as a random effect in the model. In addition: (a) models with cortical thickness as a predictor included hemisphere as a covariate, and (b) models with OCT metrics (RNFLT and GCIPLT) as a predictor included number of ON events and disease modifying therapies (DMT) as a covariate. The variance inflation factors (VIF) for all predictor variables in the model were calculated to check for multi-collinearity. All calculated VIFs were below the common threshold, thus no parameters were excluded due to collinearity (O'Brien, 2007). Individual predictors were mean centred to facilitate model convergence prior to model fitting. Normality of model residuals were checked to confirm goodness of fit and residuals were plotted to ensure homoscedasticity prior to using results in the final model. Final model selection was decided using Bayesian Information Criterion (BIC). Correction for multiple comparisons was conducted using the false discovery rate method with a threshold of 0.05.

4. Results

4.1. Demographics, OCT, and lesion volumes

Table 1 provides participant clinical and demographic characteristics. Patient and TDC did not significantly differ in sex or TIV, while patient groups did not significantly differ in time since diagnosis, EDSS, number of clinical events, DMT, total number of ON episodes or the time between last ON episode and OCT acquisition. MS patients were older at study enrolment than MOGAD patients ($p = 1.0e-04$; Table 1) and age of first symptom onset of MOGAD patients was earlier than MS patients ($p = 4.0e-05$; Supplementary Fig. 1).

MOGAD patients had significantly lower average RNFLT than TDC ($p = 7.8e-05$), yet RNFLT of MS patients did not significantly differ from TDC ($p = 0.134$) or MOGAD ($p = 0.117$). GCIPLT was lower in MOGAD patients compared to TDC ($p = 2.4e-05$), but GCIPLT of MS patients did not significantly differ from TDC ($p = 0.133$) or MOGAD ($p = 0.065$). Boxplots of age (A), age of onset (B), TIV (C), RNFLT (D) and GCIPLT for each group are available in Supplementary Fig. 1.

All MS patients (18/18) had lesions found throughout the brain compared to 11/14 MOGAD patients with lesions distributed throughout the brain. Total lesion volume differed between MS and MOGAD patients (2546mm^3 *vs.* 68mm^3, p = 2.75e-06). 13/18 MS patients had lesions within the optic radiation compared to 2/14 MOGAD patients. Lesion volume in the optic radiation among MS patients was greater than MOGAD patients (516mm^3 *vs.* 130mm^3, $p = 5.77e-03$).

4.2. Measuring differences in white matter using whole brain FBA

Fixel based differences between patients and TDC are shown in Fig. 1. On average MS patients displayed lower FD compared to TDC (Table 2). These differences were observed within multiple focal portions of the splenium, CST, fornix, corpus collosum, pons, medulla, and bilateral inferior longitudinal fasciculus (ILF) (Fig. 1, A: top panel - FD). In contrast, MS patients had fewer FC fixels that were significantly lower compared to TDC. These FC differences were observed primarily in the left CST (Fig. 1, A: middle panel - FC). While microstructural FD and macrostructural FC differences overlapped across some fibre tracts, microstructural differences were more pronounced along projection fibres, such as CST, and appeared in both hemispheres. Finally, when macro- and microstructural fibre differences were taken together in the FDC metric, MS patients demonstrated lower total intra-axonal volume occupied by fibre bundles in projection fibres (e.g., CST, brainstem, and optic radiation) and association fibres (e.g., ILF) in comparison to TDC (Fig. 1, A: bottom panel - FDC).

Fewer differences in fixel metrics were observed between MOGAD patients and TDC. MOGAD patients demonstrated lower FD within the right optic radiation only, specifically within the medial section extending to the cortex (Fig. 1, B: top panel - FD). MOGAD patients and TDC did not differ in fibre-bundle cross-section (FC). Finally, MOGAD patients demonstrated lower FDC in the right optic radiation and splenium compared to TDC (Fig. 1, B: bottom panel - FDC). Furthermore,

Table 1
Clinical and demographic characteristics: for children and adolescents with recurrent demyelinating syndromes, including multiple sclerosis (MS) and myelin oligodendrocyte glycoprotein associated disorders (MOGAD). Table also includes characteristics of typically developing children (TDC) group. (OCT: optical coherence tomography). Table include mean values and standard deviations in brackets. *p*-values were adjusted using Bonferroni.

	MS	MOGAD	TDC	*H-statistic*	*Chi-square*	*p*-value
n	18	14	26			
Sex (female/male)	12/6	11/3	16/10	–	1.2	0.55
Age at Assessment (years)	16.8(1.1)	11.8(2.8)	14.8(2.6)	16.10	–	**3.2e-04**
Range	(14.2–18.1)	(7.5–17.8)	(9.1–19.1)			
Time since diagnosis (years)	2.4(2.7)	3.0(2.1)	–	0.03	–	0.87
Range	(0.1–6.1)	(0.5–11.7)	–			
Age of Onset (years)	14.4(1.6)	10.5(3.4)	–	16.83	–	**4.0e-05**
Range	(11.7–17.4)	(2.9–13.8)				
Number of Clinical Events	2.1(1.5)	2.8 (2.3)	–	–	10.7	0.10
Range	(1–5)	(1–9)	–			
Number of Optic Neuritis Episodes (ON)	0.6(0.7)	1.1(0.8)	–	–	6.4	0.09
Range	(0–2)	(0–3)	–	–	–	–
Unilateral ON	6	1	–	–	–	–
Bilateral ON	–	10	–	–	–	–
Time between ON and OCT (years)	0.6(1.6)	0.64(1.2)	–	0.16	–	0.69
Range	(0.2–3.9)	(0.45–3.6)				
Expanded disability status scale (EDSS)	1.5	1.0	–		7.0	0.2
Range	(0–4.5)	(0–3)	–			
Disease Modifying Therapies	11/18	8/14	–		0.87	0.83
Total intracranial volume (cm^3)	1373(29)	1382(42)	1440(28.7)	59	–	0.48
Range	(1148–1587)	(986–1609)	(1131–1715)			
Lesion Volume (mm^3)	2546(1972)	68.0(567)	–	10.8	–	**1.0e-03**
Range	(0–35046)	(0–7998)	–			
Retinal Nerve Fibre Layer Thickness (μm)	86.5(13.6)	78(16.7)	95.5(10.7)	18.0	–	**1.3e-04**
Range	(66–110)	(49–99)	(82–126)			
Ganglion Cell Layer Thickness (μm)	76.2(11.9)	64.9(12.0)	84.4(5.12)	20.1	–	**4.3e-5**
Range	(54–91)	(51–86)	(70–92)			
Time between Steroid treatment and MRI (years)	3.8(3.12)	2.2(3.3)	–			–
Time between Disease Modifying Therapy and MRI (years)	1.19(1.81)	0.53(2.72)	–			–

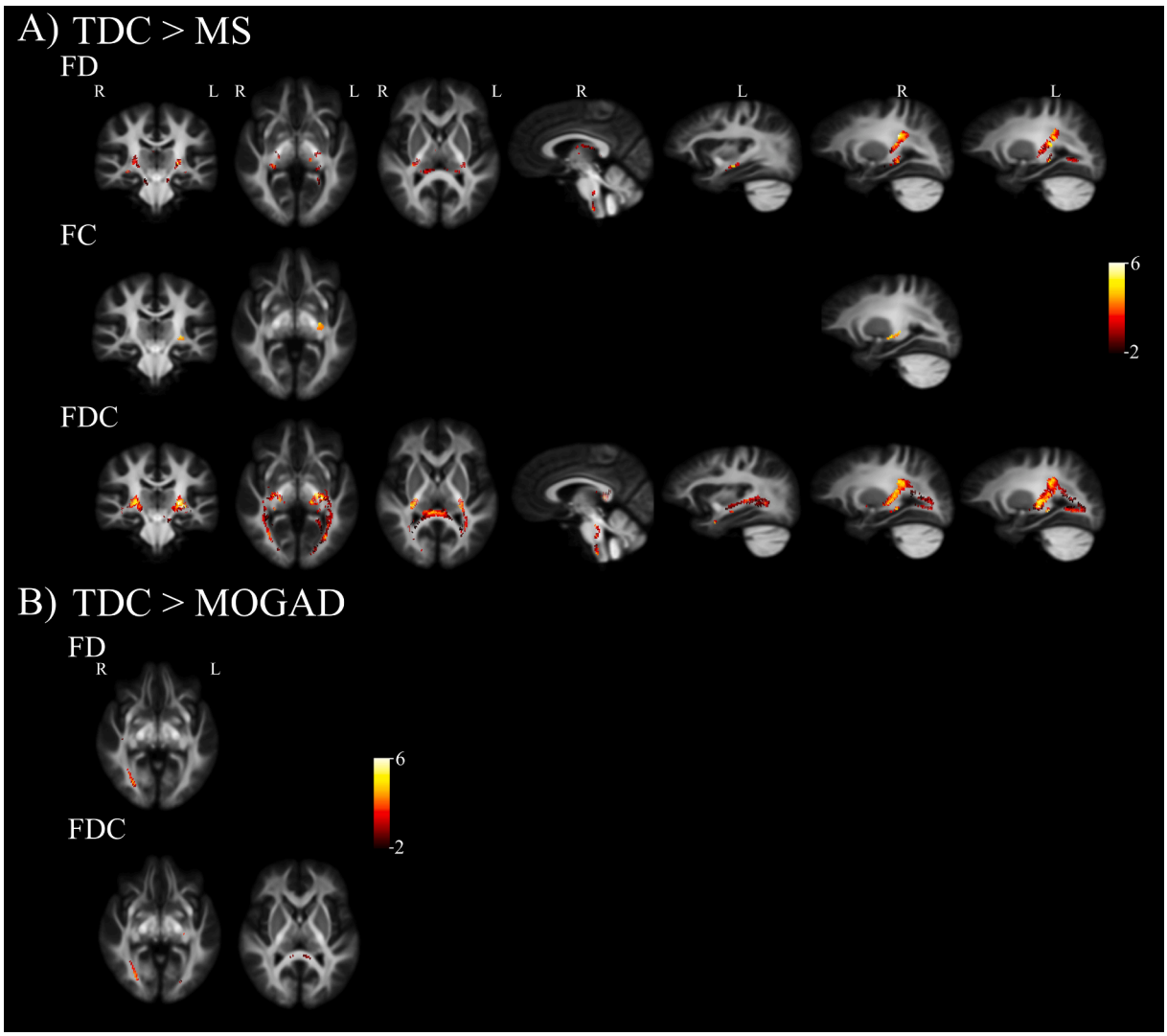

Fig. 1. Whole-brain fixel-based analysis (FBA) revealed reductions in fixel metrics for paediatric patients with demyelinating syndromes when compared to typically developing children (TDC). All maps are superimposed on a study-specific template and colour-coded by effect size (F-statistic, thresholded at FWE-p < 0.05). Analysis accounted for effects of sex, age, and total intracranial volume. (A) MS patients revealed reductions in fibre density (FD), fibre-bundle cross section (FC) and fibre-density and fibre-bundle cross-section (FDC) when compared to TDC (B) MOGAD patients revealed reductions in FD and FDC when compared to TDC.

when lesion free MOGAD patients (3/14) were excluded from fixel analysis the right optic radiation was the only area that passed multiple comparisons.

4.3. Measuring differences in grey matter using cortical thickness analysis

We observed a group effect within TDC, MS and MOGAD participants using an ANOVA in cortical thickness within frontal, visual and parietal cortices ($p < 0.001$) (Supplementary Fig. 2). In post hoc analysis, MS patients had lower cortical thickness in frontal, temporal (right hemisphere) and parietal (left hemisphere) cortices compared to TDC ($p < 0.05$, TFCE-corrected; Fig. 2A). While MS patients had similar cortical thickness to TDC within the visual cortex, MOGAD patients demonstrated a significantly thinner cortex within V1 ($p < 0.05$, TFCE-correct; Fig. 2B) compared to TDC. MOGAD patients also demonstrated a significantly thinner cortices in the frontal lobe and anterior cingulate cortex (ACC) compared to TDC (Fig. 2B). When including MOGAD patients with and without lesions, we saw no difference in cortical areas with significant thinning. No significant differences in cortical thickness were evident between MS and MOGAD patients.

4.4. Measuring white matter within the optic radiations.

Mean FD, FC, FDC, AWF and TORT values differed between patients and TDC within normal appearing WM (NAWM) of the optic radiations (Table 2). Pairwise Dunn tests demonstrated lower fixel metrics (FD, FC and FDC) in both MOGAD and MS patients compared to TDC (Table 2). MS and MOGAD patients also displayed lower TORT than TDC ($p = 7.8e\text{-}09$ and $p = 3.8e\text{-}06$, respectively). All three groups had similar mean AWF values within the NAWM of the optic radiations (Table 2). Finally, the two patient groups did not differ from each other in any of the fixel metrics or TORT (Table 2).

4.5. Predictive models of optic radiation using V1 cortical thickness and OCT in patient groups

In the MS group, reduced V1 cortical thickness measures predicted lower FC ($p = 0.015$) and TORT ($p = 0.05$) along the optic radiation, after adjusting for age, sex, and time since diagnosis (Table 3; Supplementary Fig. 2). There were no significant relationships between V1 cortical thickness and FD, FDC or AWF in MS patients, after adjusting for age, sex, and time since diagnosis (Table 3). In the MOGAD group, no

Table 2
Comparison of the optic radiation diffusion metrics between typically developing children (TDC) and children and adolescents with recurrent demyelinating syndromes, including patients with multiple sclerosis (MS) and myelin oligodendrocyte glycoprotein associated disorders (MOGAD). Diffusion metrics: fibre density (FD), fibre cross-section (FC), fibre density and cross-section (FDC), axonal water fraction (AWF) and tortuosity (TORT). *p*-values were adjusted using false discovery rate (FDR).

Metrics	MS	MOGAD	TDC	*H-statistic*	*p*-value
FD	0.421 (0.007)	0.416 (0.008)	0.45 (0.003)	32.9	**<0.001**
				−4.69	**<0.001**
				−4.82	**<0.001**
				0.21	0.8
FC	−0.026 (0.019)	0.011 (0.029)	0.094 (0.017)	21.0	**0.00003**
				−3.35	**0.0012**
				−4.16	**0.000095**
				−0.466	0.64
FDC	0.419 (0.012)	0.529 (0.015)	0.482 (0.009)	31.5	**<0.001**
				−4.38	**0.000018**
				−4.91	**0.0000027**
				−0.152	0.88
AWF	0.341 (0.003)	0.346 (0.003)	0.347 (0.002)	5.73	0.056
				−0.348	0.728
				−2.32	0.06
				−1.68	0.094
TORT	2.11 (0.039)	2.15 (0.042)	2.39 (0.017)	43.3	**<0.001**
				−4.84	**0.0000038**
				−5.95	**0.0000000078**
				−0.616	1

significant relationships were found between V1 cortical thickness and any fixel or WMTI metrics (Table 3; Supplementary Table 2).

In the MS group, lower RNFLT predicted lower TORT within the optic radiation ($p = 0.034$), after adjusting for age, sex, time since diagnosis and number of ON events (Table 4; Supplementary Figure 4). There was no significant relationship between RNFLT and FD, FC, FDC or AWF in MS patients, after adjusting for age, sex, time since diagnosis and number of ON events. In the MOGAD group, lower RNFLT predicted lower FC ($p = 0.041$) (Table 4, Supplementary Figure 4), after adjusting for age, sex, time since diagnosis and number of ON episodes. In contrast, lower RNFLT predicted higher AWF ($p = 0.047$) in MOGAD patients (Supplementary Figure 4), after adjusting for age, sex, and time since diagnosis. We found no significant relationship between RNFLT and diffusion metrics (FD, FDC and TORT) in MOGAD patients after adjusting for age, sex, time since diagnosis and number of ON events. Models including number of ON events as a covariate did not produce a better fit for all models except for FC in MOGAD patients (Supplementary Tables 3 and 4). There was no significant relationship between GCIPLT and all diffusion metrics (FD, FC, FDC, AWF and TORT) in both MS and MOGAD patients, after adjusting for age, sex, time since diagnosis and number of ON events (Supplementary Tables 5 and 6).

5. Discussion

This is the first study to evaluate the visual pathway from anterior (retina) to posterior (visual cortex) regions in both paediatric MOGAD and MS patients. In this study, we found differences in the voxel-wise and fixel-based MRI parameters evaluated in both MS and MOGAD patients when compared with TDC. First, compared to TDC, MS patients showed evidence of (a) multiple discrete areas of reduced FD including the CST and ILF, and (b) decreased cortical thickness in the parietal and temporal cortices. Second, compared to TDC, MOGAD patients showed evidence of (a) reduced FD localized to optic radiation, and (b) decreased cortical thickness in the visual, superior frontal and cingulate cortices. When we solely focused on the optic radiations in a region of interest analysis, we observed reduced FD and lower TORT (an estimate of myelin volume) in both patient groups relative to TDC.

Notably, in the MS group, but not the MOGAD group, reduced cortical thickness in the visual cortex predicted lower FC and TORT in the optic radiations. With regards to measures of retinal atrophy, RNFLT predicted lower FC in the optic radiations in MOGAD and lower TORT in MS patients. Implications of these findings are discussed below.

5.1. White matter damage in paediatric demyelinating disorders measured using FBA

Our findings are consistent with previous DTI work demonstrating that children and adolescents with demyelinating syndromes (i.e., MS, acquired demyelinating syndrome and acute disseminated encephalomyelitis) display compromise in normal-appearing white matter (Akbar et al., 2016; Longoni et al., 2017). Here, we extend this work using whole brain fixel-based measures to assess specific fibre-bundle micro- and macrostructural changes within our patient population when compared to TDC. White matter injury or loss is characterized by decreases in FD, FC, and the combination of the two (FDC). A decrease in FD suggests a decrease in intra-axonal volume fraction, meaning that the fraction of space occupied by the axons is smaller within a voxel. Smaller intra-axonal volume fractions may be caused by axons decreasing in diameter or axonal loss (i.e., fewer axons occupying this space). We found regional decreases in FD across multiple white matter pathways, namely in the CST, brainstem tracts, ILF, and optic radiations in MS patients. When we ran the analysis excluding the single MS patient that was scanned<3 months (0.22 years) from their acute optic neuritis and clinical event, we saw no difference in fixel and WMTI metrics. In MOGAD patients, on the other hand, differences were limited to the optic radiations. When including MOGAD patients with and without lesions, we also saw a difference in the splenium. Consistent with previous diffusion studies in paediatric MS (Datta et al., 2019) and MOGAD (Bells et al., 2019) populations and in line with our hypotheses, we observed lower FD and FDC within the visual pathway in both patient populations compared to TDC. Few differences from TDC were observed in FC in our MS or MOGAD patients.

In TDC, increased axonal packing reflects age-related maturation in the CST and ILF microstructure (Chang et al., 2015; Dimond et al., 2020; Lebel and Deoni, 2018). We observed lower FD within the CST in MS patients when compared to TDC, whereas no differences in the CST were seen in a previous DTI study (Waldman et al., 2020). This may relate to the higher tissue specificity of FBA *vs* DTI metrics. Consistent with a previous adult MS study, we found decreased FD and FDC within the ILF in MS patients (Gajamange et al., 2018). Overall, our FBA demonstrated widespread FD reduction in paediatric MS patients, while regional FD loss, mainly in the posterior visual pathway, was evident in MOGAD patients.

5.2. Cortical thinning in paediatric demyelinating disorders

Consistent with previous studies of adults with MS (Steenwijk et al., 2016; Tsagkas et al., 2020) and in children and adolescents (Muthuraman et al., 2020; Tsagkas et al., 2020), we observed reduced cortical thickness in the temporal poles. We also observed reduced cortical thickness in superior frontal cortex and parietal cortex. The reasons for the observed thinning demonstrated in the temporal pole and precentral-gyrus in our cross-sectional study are unknown: other literature suggests that thinning may represent a combination of a disease-specific effect and altered growth trajectory, as grey matter regions develop non-linearly (Gogtay et al., 2004; Vijayakumar et al., 2016) and have unique growth trajectories (Tamnes et al., 2017; Wierenga et al., 2014). Supporting this, a longitudinal study in children with MS (De Meo et al., 2019) suggested cortical thinning was associated with (1) altered growth trajectory in frontal, temporal, parietal, and occipital

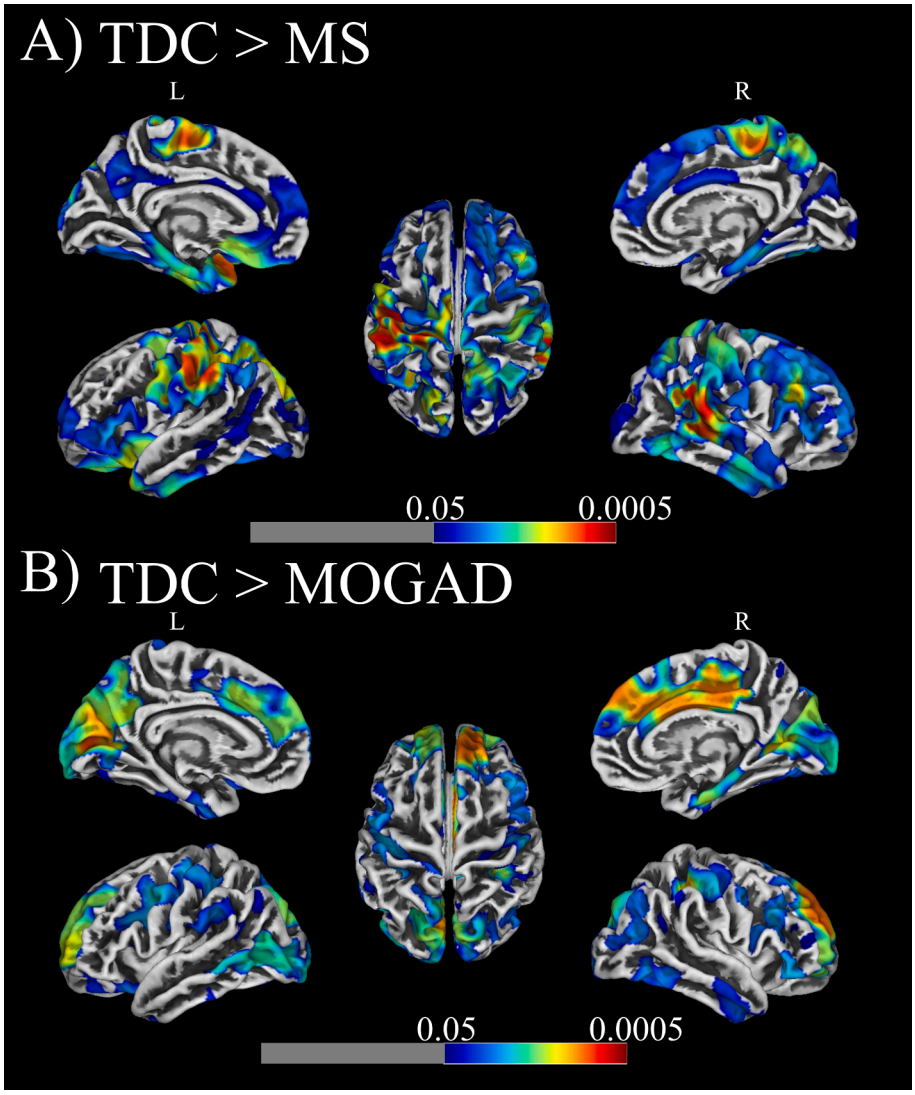

Fig. 2. Surface-based morphometry analysis revealed reductions in cortical thickness for (A) MS and (B) MOGAD patients when compared to typically developing children (TDC). Results were thresholded at voxel level with $p < 0.05$ and corrected with cluster level non-stationary cluster extent and superimposed on a template reconstruction of brain surface in MNI space. Analysis accounted for effects of sex and age.

Table 3
Results from linear mixed effects models including cortical thickness. The lmer function automatically performed t-tests using Satterthwaite approximations to estimate degrees of freedom. Values describe relationships between diffusion white matter measures (FD, FC, FDC, AWF and TORT) and grey matter cortical thickness (CTh) measures in MS and MOGAD patients. (FD: fibre density, FC: fibre cross-section, FDC: fibre density and cross-section, AWF: axonal water fraction, TORT: tortuosity).

Patient Group	WM metrics	CTh	CI (95%)	p_{adj}-value
MS	FD	0.011	−0.006,0.028	0.22
MOGAD	FD	0.003	−0.011,0.016	0.71
MS	FC	0.048	0.012,0.084	**0.015**
MOGAD	FC	0.030	−0.014,0.075	0.20
MS	FDC	0.021	−0.007,0.049	0.15
MOGAD	FDC	0.011	−0.014,0.036	0.39
MS	AWF	0.004	−0.004,0.012	0.35
MOGAD	AWF	0.005	−0.003,0.012	0.24
MS	TORT	0.082	0.003,0.160	**0.051**
MOGAD	TORT	0.026	−0.034,0.089	0.43

Table 4
Results from linear mixed effects models including retinal nerve fibre layer thickness. The lmer function automatically performed t-tests using Satterthwaite approximations to estimate degrees of freedom. Values describe relationships between diffusion white matter measures (FD, FC, FDC, AWF and TORT) and retinal nerve fibre layer thickness (RNFLT) measures in MS and MOG patients. (FD: fibre density, FC: fibre cross-section, FDC: fibre density and cross-section, AWF: axonal water fraction, TORT: tortuosity).

Patient Group	WM metrics	RNFLT	CI (95%)	p_{adj}-value
MS	FD	0.017	−0.0045,0.039	0.15
MOGAD	FD	0.007	0.037,0.46	0.66
MS	FC	0.028	−0.042,0.097	0.46
MOGAD	FC	0.007	0.017,0.14	**0.041**
MS	FDC	0.002	−0.015,0.071	0.22
MOGAD	FDC	0.036	−0.0058,0.078	0.13
MS	AWF	0.002	−0.012,0.015	0.80
MOGAD	AWF	−0.014	−0.024,-0.0050	**0.020**
MS	TORT	0.130	0.022,0.23	**0.037**
MOGAD	TORT	0.059	−0.093,0.21	0.47

poles; (2) white matter lesions in highly connected cortical areas that develop later, such as anterior fronto-temporal regions and to a lesser extent the precentral-gyrus; and (3) time since diagnosis (Ziegler et al., 2017). We found no differences in cortical thickness within the primary visual cortex (i.e., V1) between MS patients and TDC, which will be discussed below in the context of relations with the rest of the visual pathway (i.e., optic radiations and retinal thickness). Longitudinal studies with larger cohorts are needed to fully understand the relationship between altered cortical thickness, disease-specific effect, and growth trajectory.

5.3. Comparing white matter, cortical thickness, and retinal nerve fibre layer thickness in the visual system

Although we did not observe differences in cortical thickness within the primary visual cortex (V1) of MS patients compared to TDC, MS patients exhibited lower FC and TORT within the optic radiations, which were associated with thinner V1 cortex. Our results are consistent with previous paediatric MS studies showing that lower cortical thickness in the visual cortex correlates with diffusion tensor metrics (Datta et al., 2019; Waldman et al., 2020) and provide further evidence linking abnormal structure within the optic radiation and cortex. The lack of a significant relationship between FD within the optic radiation and cortical thickness in the visual cortex of MOGAD patients may indicate white matter injury to the visual pathway may not have long term consequences on the visual cortex and/or that other factors are relevant here. Such as, reorganisation of V1 after injury that can only be determined from retinotopic mapping within each patient.

Despite finding no significant differences between MS patients and TDC in RNFLT, we found abnormalities within the optic radiation to be significantly associated with thickness of the RNFL in these patients. Our findings add to a growing body of research suggesting a relationship between RNFLT and white matter compromise in paediatric MS patients (Datta et al., 2019; Waldman et al., 2020). While previous studies have shown RNFLT abnormalities in children with MOGAD (Eyre et al., 2018; Song et al., 2019), the relationship between structural MRI metrics, specifically in the optic radiations, has not yet been elucidated. Others have shown associations between RNFLT, optic radiation abnormalities and cortical thickness in adult and paediatric patients with MS and have noted these abnormalities associated primarily with the presence of ON (Balk et al., 2015; Chen et al., 2018; Datta et al., 2019; Klistorner et al., 2014; Ngamsombat et al., 2020). In our MOGAD cohort, the association between optic radiation FC and RNFLT is consistent with these studies and might support *trans*-synaptic degeneration of the *retro*-geniculate visual pathways secondary to ON (Eyre et al., 2018). Notably, RNFL thinning predicted lower FC in the optic radiation, even after accounting for ON episodes, hinting at the presence of ongoing pathological processes above and beyond the acute inflammatory insult. Interestingly, in our MOGAD patient group we found that lower RNFLT predicted higher AWF. A decrease in AWF is thought to reflect axonal degeneration (de Kouchkovsky et al., 2016), but has been shown to increase due to an acute inflammatory demyelinating phase associated with extensive infiltration and proliferation of microglia (Guglielmetti et al., 2016). This may represent low grade, ongoing inflammation, which is currently undetectable using conventional MRI, or, alternatively, the dynamic changes related to acute inflammation in the recovery phase, as we included some patients as 30 days after an episode of ON. Longitudinal studies are needed to gain clarity on this relationship.

Despite finding differences between MOGAD patients and TDC in GCIPLT, we found abnormalities within the optic radiation were not significantly associated with thickness of the GCIPL in these patients. Furthermore, in our MS patient group no significant association was found between GCIPLT and WM structural abnormalities within the optic radiation.

5.4. Limitations and future directions

Limitations of this study include its cross-sectional design, the small sample size, and heterogeneity in factors such as disease modifying therapies (DMT) and number of ON episodes within the two patient populations. Unfortunately, due to the cross-sectional design of the study and the clinical presentation of multiple ON episodes in some patients, it would be difficult to use clinical markers such as visual acuity at nadir or EDTs in our current study. Future studies that include these measures across the course/duration of the patient's disease would be needed. We note that the results provide insights into axonal abnormalities in these populations, though the small population limits generalizability. However, we highlight that despite the small sample size; we observed differences in fixel metrics specifically along the optic radiation, which may be of pathological significance in these disorders. Due to known age-related factors, we were careful to perform our analyses using age- and sex-matched controls. Both the fixel and cortical thickness analysis were performed using age- and sex-matched controls and age was used as a covariate in these analyses. Furthermore, NAWM can be downstream or upstream from lesions in WM tracts, and therefore affected by anterograde or retrograde axonal degeneration. Future studies are needed to separate NAWM into tracts affected by lesions (with lesions themselves removed) and tracts unaffected by lesions. In our linear mixed models, predictors of cortical thickness were FC and TORT in MS patients but not in MOGAD related disorders, likely due to the relatively small sample of MOGAD patients. Furthermore, when evaluating fixel data we interpreted loss of FD as a proxy for axonal loss, and decreased FC as a proxy for shrinkage of the fibre bundle. However, other processes such as inflammation and edema could confound or dilute the relationship between WMTI and FBA measures, thus, to improve interpretability validated both measures against direct measurements of axons and myelin (i.e., through animal models) are needed. Furthermore, longitudinal studies that measure WMTI and fixel metrics along disease progression are needed to understand the effect MS and MOGAD have on these measures and how they correspond to OCT RNFLT along the patient's disease course. These analyses were beyond the scope of this clinical cohort comparison study.

Finally, longitudinal studies will help clarify the relationship between abnormalities in optic radiation axons and visual cortex in children and adolescents with demyelinating disorders.

6. Conclusion

We found different white and grey matter microstructure abnormalities in children and adolescents with MS and MOGAD. MS patients exhibited more widespread white matter abnormalities; MOGAD patients exhibited white matter changes primarily within the optic radiation. Furthermore, the pattern of cortical thinning differed in MS and MOGAD patients: it was seen in the temporal and parietal areas in MS patients, and the cingulate, frontal, and visual cortices in patients with MOGAD related disorders. Finally, our findings of associations between lower RNFLT and axonal integrity in both MS and MOGAD patients when compared to TDC in the optic radiations suggest widespread axonal and myelin damage in the visual pathway. This may be associated with cortical thinning in MOGAD patients. Our approach of combining FBA, cortical thickness and RNFLT measures – white and grey matter markers – has helped to distinguish patterns of structural abnormality associated with MS and MOGAD patients. Future longitudinal studies should focus on characterising clinical trajectories of each disorder, identifying distinct phenotypes and their impact on developmental plasticity, and leveraging biomarkers to improve clinical practice and treatment.

CRediT authorship contribution statement

Sonya Bells: Conceptualization, Methodology, Software, Validation,

Formal analysis, Data curation, Writing – original draft, Writing – review & editing. **Giulia Longoni:** Conceptualization, Methodology, Data curation, Writing – original draft, Writing – review & editing. **Tara Berenbaum:** Investigation, Resources, Data curation, Writing – review & editing, Project administration. **Cynthia B. de Medeiros:** Investigation, Resources, Data curation, Writing – review & editing, Project administration. **Sridar Narayanan:** Resources, Writing – review & editing. **Brenda L. Banwell:** Funding acquisition, Writing – review & editing. **Douglas L. Arnold:** Resources, Funding acquisition, Writing – review & editing. **Donald J. Mabbott:** Conceptualization, Methodology, Validation, Resources, Writing – review & editing, Supervision, Funding acquisition. **E. Ann Yeh:** Conceptualization, Methodology, Validation, Resources, Writing – review & editing, Supervision, Funding acquisition.

Declaration of Competing Interest

The authors declare that they have no known competing financial interests or personal relationships that could have appeared to influence the work reported in this paper.

Acknowledgements

The authors thank Stephanie Grover, Danusha Nandamalavan, and Austin Noguera for their assistance with participant recruitment and Jovanka Skocic, Tammy Rayner, and Ruth Weiss for image acquisition. We would like to thank Julia O'Mahony, Olivia Lau, Rozie Arnaoutelis and Samson Antel for their work in MRI data organisation and database creation for the National study component of this database. We would also like to thank Els Fieremans and Benjamin Ades-Aron at New York University for their invaluable help in applying the DESIGNER pipeline. This research was supported by the Ontario Institute for Regenerative Medicine (OIRM grant to D.J.M. and A.E.Y.), Canadian MS Research Foundation funding (A.E.Y, B.B. and D.L.A.) and Canadian Stem Cell Network (DMT12 Miller: A.E.Y and D.J.M). S.B. was supported by Restracomp from the Research Institute and the Nate and Selina Bresver Fellowship from Centre for Brain & Mental Health at the Hospital for Sick Children.

Appendix A. Supplementary data

Supplementary data to this article can be found online at https://doi.org/10.1016/j.nicl.2022.103001.

References:

Ades-Aron, B., Veraart, J., Kochunov, P., McGuire, S., Sherman, P., Kellner, E., Novikov, D.S., Fieremans, E., 2018. Evaluation of the accuracy and precision of the diffusion parameter EStImation with Gibbs and NoisE removal pipeline. Neuroimage 183, 532–543. https://doi.org/10.1016/j.neuroimage.2018.07.066.

Akbar, N., Giorgio, A., Till, C., Sled, J.G., Doesburg, S.M., De Stefano, N., Banwell, B., Yap, P.-T., 2016. Alterations in functional and structural connectivity in pediatric-onset multiple sclerosis. PLoS ONE 11 (1), e0145906.

Aliotta, R., Cox, J.L., Donohue, K., Weinstock-Guttman, B., Yeh, E.A., Polak, P., Dwyer, M.G., Zivadinov, R., 2014. Tract-based spatial statistics analysis of diffusion-tensor imaging data in pediatric- and adult-onset multiple sclerosis. Hum. Brain Mapp. 35, 53–60. https://doi.org/10.1002/hbm.22148.

Andersson, J.L.R., Skare, S., Ashburner, J., 2003. How to correct susceptibility distortions in spin-echo echo-planar images: Application to diffusion tensor imaging. Neuroimage 20, 870–888. https://doi.org/10.1016/S1053-8119(03)00336-7.

Andersson, J.L.R., Sotiropoulos, S.N., 2016. An integrated approach to correction for off-resonance effects and subject movement in diffusion MR imaging. Neuroimage 125, 1063–1078. https://doi.org/10.1016/j.neuroimage.2015.10.019.

Assaf, Y., Basser, P.J., 2005. Composite hindered and restricted model of diffusion (CHARMED) MR imaging of the human brain. Neuroimage 27, 48–58. https://doi.org/10.1016/j.neuroimage.2005.03.042.

Aung, W.Y., Massoumzadeh, P., Najmi, S., Salter, A., Heaps, J., Benzinger, T.L.S., Mar, S., 2018. Diffusion Tensor Imaging as a Biomarker to Differentiate Acute Disseminated Encephalomyelitis From Multiple Sclerosis at First Demyelination. Pediatr. Neurol. 78, 70–74. https://doi.org/10.1016/j.pediatrneurol.2017.09.016.

Avants, B.B., Tustison, N.J., Stauffer, M., Song, G., Wu, B., Gee, J.C., 2014. The Insight ToolKit image registration framework. Front. Neuroinform. 8, 1–13. https://doi.org/10.3389/fninf.2014.00044.

Balk, L.J., Steenwijk, M.D., Tewarie, P., Daams, M., Killestein, J., Wattjes, M.P., Vrenken, H., Barkhof, F., Polman, C.H., Uitdehaag, B.M.J., Petzold, A., 2015. Bidirectional trans-synaptic axonal degeneration in the visual pathway in multiple sclerosis. J. Neurol. Neurosurg. Psychiatry 86, 419–424. https://doi.org/10.1136/jnnp-2014-308189.

Basser, P.J., Pierpaoli, C., 1996. Microstructural and physiological features of tissues elucidated by quantitative-diffusion-tensor MRI. J Magn Reson B 111 (3), 209–219.

Bates, D., Mächler, M., Bolker, B., Walker, S., 2014. Fitting linear mixed-effects models using lme4. J. Stat. Softw. 67, 1–48.

Beaulieu, C., 2002. The basis of anisotropic water diffusion in the nervous system - a technical review. NMR Biomed 15, 435–455. https://doi.org/10.1002/nbm.782.

Beaulieu, C., Allen, P.S., 1994. Water diffusion in the giant axon of the squid: implications for diffusion-weighted MRI of the nervous system. Magn Reson Med 32 (5), 579–583.

Bells, S., Lefebvre, J., Longoni, G., Narayanan, S., Arnold, D.L., Yeh, E.A., Mabbott, D.J., 2019. White matter plasticity and maturation in human cognition. Glia 67 (11), 2020–2037.

Bennett, J.L., de Seze, J., Lana-Peixoto, M., Palace, J., Waldman, A., Schippling, S., Tenembaum, S., Banwell, B., Greenberg, B., Levy, M., Fujihara, K., Chan, K.H., Kim, H.J., Asgari, N., Sato, D.K., Saiz, A., Wuerfel, J., Zimmermann, H., Green, A., Villoslada, P., Paul, F., 2015. Neuromyelitis optica and multiple sclerosis: Seeing differences through optical coherence tomography. Mult. Scler. J. 21 (6), 678–688.

Bergsland, N., Horakova, D., Dwyer, M.G., Dolezal, O., Seidl, Z.K., Vaneckova, M., Krasensky, J., Havrdova, E., Zivadinov, R., 2012. Subcortical and cortical gray matter atrophy in a large sample of patients with clinically isolated syndrome and early relapsing-remitting multiple sclerosis. Am. J. Neuroradiol. 33, 1573–1578. https://doi.org/10.3174/ajnr.A3086.

Calabrese, M., Atzori, M., Bernardi, V., Morra, A., Romualdi, C., Rinaldi, L., McAuliffe, M.J.M., Barachino, L., Perini, P., Fischl, B., Battistin, L., Gallo, P., 2007. Cortical atrophy is relevant in multiple sclerosis at clinical onset. J. Neurol. 254, 1212–1220. https://doi.org/10.1007/s00415-006-0503-6.

Chang, Y.S., Owen, J.P., Pojman, N.J., Thieu, T., Bukshpun, P., Wakahiro, M.L.J., Berman, J.I., Roberts, T.P.L., Nagarajan, S.S., Sherr, E.H., Mukherjee, P., Gong, G., 2015. White matter changes of neurite density and fiber orientation dispersion during human brain maturation. PLoS ONE 10 (6), e0123656.

Chen, J.J., Flanagan, E.P., Jitprapaikulsan, J., López-Chiriboga, A.(.S., Fryer, J.P., Leavitt, J.A., Weinshenker, B.G., McKeon, A., Tillema, J.-M., Lennon, V.A., Tobin, W. O., Keegan, B.M., Lucchinetti, C.F., Kantarci, O.H., McClelland, C.M., Lee, M.S., Bennett, J.L., Pelak, V.S., Chen, Y., VanStavern, G., Adesina, O.-O., Eggenberger, E. R., Acierno, M.D., Wingerchuk, D.M., Brazis, P.W., Sagen, J., Pittock, S.J., 2018. Myelin Oligodendrocyte Glycoprotein Antibody-Positive Optic Neuritis: Clinical Characteristics, Radiologic Clues, and Outcome. Am. J. Ophthalmol. 195, 8–15.

Chuhutin, A., Hansen, B., Wlodarczyk, A., Owens, T., Shemesh, N., Jespersen, S.N., 2020. Diffusion Kurtosis Imaging maps neural damage in the EAE model of multiple sclerosis. Neuroimage 208, 116406.

Ciftci-Kavaklioglu, B., Yeh, E.A., 2020. Evaluating visual outcomes using optical coherence tomography (OCT) in pediatric multiple sclerosis and other neuroinflammatory conditions. Ann. Eye Sci. 5, 16–16. doi:10.21037/aes.2020.02.03.

Collier, Q., Veraart, J., Jeurissen, B., Den Dekker, A.J., Sijbers, J., 2015. Iterative reweighted linear least squares for accurate, fast, and robust estimation of diffusion magnetic resonance parameters. Magn. Reson. Med. 73, 2174–2184. https://doi.org/10.1002/mrm.25351.

Dahnke, R., Yotter, R.A., Gaser, C., 2013. Cortical thickness and central surface estimation. Neuroimage 65, 336–348. https://doi.org/10.1016/j.neuroimage.2012.09.050.

Datta, R., Sollee, J.R., Lavery, A.M., Ficerai-Garland, G., Karoscik, K., Liu, G., Banwell, B. L., Waldman, A.T., 2019. Effects of Optic Neuritis, T2 Lesions, and Microstructural Diffusion Integrity in the Visual Pathway on Cortical Thickness in Pediatric-Onset Multiple Sclerosis. J. Neuroimaging 29, 760–770. https://doi.org/10.1111/jon.12654.

de Kouchkovsky, I., Fieremans, E., Fleysher, L., Herbert, J., Grossman, R.I., Inglese, M., 2016. Quantification of normal-appearing white matter tract integrity in multiple sclerosis: a diffusion kurtosis imaging study. J. Neurol. 263, 1146–1155. https://doi.org/10.1007/s00415-016-8118-z.

De Meo, E., Meani, A., Moiola, L., Ghezzi, A., Veggiotti, P., Filippi, M., Rocca, M.A., 2019. Dynamic gray matter volume changes in pediatric multiple sclerosis: A 3.5 year MRI study. Neurology 92, e1709–e1723. https://doi.org/10.1212/WNL.0000000000007267.

De Meo, E., Storelli, L., Moiola, L., Ghezzi, A., Veggiotti, P., Filippi, M., Rocca, M.A., 2021. In vivo gradients of thalamic damage in paediatric multiple sclerosis: A window into pathology. Brain 144, 186–197. https://doi.org/10.1093/brain/awaa379.

De Stefano, N., Airas, L., Grigoriadis, N., Mattle, H.P., O'Riordan, J., Oreja-Guevara, C., Sellebjerg, F., Stankoff, B., Walczak, A., Wiendl, H., Kieseier, B.C., 2014. Clinical relevance of brain volume measures in multiple sclerosis. CNS Drugs 28, 147–156. https://doi.org/10.1007/s40263-014-0140-z.

Dell'Acqua, F., Simmons, A., Williams, S.C.R.R., Catani, M., 2013. Can spherical deconvolution provide more information than fiber orientations? Hindrance modulated orientational anisotropy, a true-tract specific index to characterize white matter diffusion. Hum. Brain Mapp. 34, 2464–2483. https://doi.org/10.1002/hbm.22080.

Dhollander, T., Mito, R., Raffelt, D., Connelly, A., 2019. Improved white matter response function estimation for 3-tissue constrained spherical deconvolution. Proc. Intl. Soc. Mag. Reson, Med, p. 555.

Dhollander, T., Raffelt, D., Connelly, A., 2017. Towards interpretation of 3-tissue constrained spherical deconvolution results in pathology. Proc. Intl. Soc. Mag. Reson, Med, p. 25.
Dhollander, T., Raffelt, D., Connelly, A., 2016. Unsupervised 3-tissue response function estimation from single-shell or multi-shell diffusion MR data..., in: ISMRM. pp. 1–2.
Dimond, D., Rohr, C.S., Smith, R.E., Dhollander, T., Cho, I., Lebel, C., Dewey, D., Connelly, A., Bray, S., 2020. Early childhood development of white matter fiber density and morphology. Neuroimage 210, 116552. https://doi.org/10.1016/j.neuroimage.2020.116552.
Elliott, C., 2016. A Bayesian Framework for 4-D Segmentation of Multiple Sclerosis Lesions in Serial MRI of the Brain. McGill Univ, McGill University.
Eyre, M., Hameed, A., Wright, S., Brownlee, W., Ciccarelli, O., Bowman, R., Lim, M., Wassmer, E., Thompson, D., Hemingway, C., Hacohen, Y., 2018. Retinal nerve fibre layer thinning is associated with worse visual outcome after optic neuritis in children with a relapsing demyelinating syndrome. Dev. Med. Child Neurol. 60, 1244–1250. https://doi.org/10.1111/dmcn.13757.
Fieremans, E., Jensen, J.H., Helpern, J.A., 2011. White matter characterization with diffusional kurtosis imaging. Neuroimage 58, 177–188. https://doi.org/10.1016/j.neuroimage.2011.06.006.
Filippi, M., Preziosa, P., Rocca, M.A., 2014. Magnetic resonance outcome measures in multiple sclerosis trials: Time to rethink? Curr. Opin. Neurol. 27, 290–299. https://doi.org/10.1097/WCO.0000000000000095.
Gajamange, S., Raffelt, D., Dhollander, T., Lui, E., van der Walt, A., Kilpatrick, T., Fielding, J., Connelly, A., Kolbe, S., 2018. Fibre-specific white matter changes in multiple sclerosis patients with optic neuritis. NeuroImage Clin. 17, 60–68. https://doi.org/10.1016/j.nicl.2017.09.027.
Geurts, J.J.G., Barkhof, F., 2008. Grey matter pathology in multiple sclerosis. Lancet Neurol 7, 841–851. https://doi.org/10.1007/978-88-470-2127-3_9.
Geurts, J.J.G., Calabrese, M., Fisher, E., Rudick, R.A., 2012. Measurement and clinical effect of grey matter pathology in multiple sclerosis. Lancet Neurol. 11, 1082–1092. https://doi.org/10.1016/S1474-4422(12)70230-2.
Gogtay, N., Giedd, J.N., Lusk, L., Hayashi, K.M., Greenstein, D., Vaituzis, A.C., Nugent, T. F., Herman, D.H., Clasen, L.S., Toga, A.W., Rapoport, J.L., Thompson, P.M., 2004. Dynamic mapping of human cortical development during childhood through early adulthood. Proc. Natl. Acad. Sci. U. S. A. 101 (21), 8174–8179.
Granberg, T., Fan, Q., Treaba, C.A., Ouellette, R., Herranz, E., Mangeat, G., Louapre, C., Cohen-Adad, J., Klawiter, E.C., Sloane, J.A., Mainero, C., 2017. In vivo characterization of cortical and white matter neuroaxonal pathology in early multiple sclerosis. Brain 140, 2912–2926. https://doi.org/10.1093/brain/awx247.
Guglielmetti, C., Veraart, J., Roelant, E., Mai, Z., Daans, J., Van Audekerke, J., Naeyaert, M., Vanhoutte, G., Delgado y Palacios, R., Praet, J., Fieremans, E., Ponsaerts, P., Sijbers, J., Van der Linden, A., Verhoye, M., 2016. Diffusion kurtosis imaging probes cortical alterations and white matter pathology following cuprizone induced demyelination and spontaneous remyelination. Neuroimage 125, 363–377.
Hagiwara, A., Kamagata, K., Shimoji, K., Yokoyama, K., Andica, C., Hori, M., Fujita, S., Maekawa, T., Irie, R., Akashi, T., Wada, A., Suzuki, M., Abe, O., Hattori, N., Aoki, S., 2019. White matter abnormalities in multiple sclerosis evaluated by quantitative synthetic MRI, diffusion tensor imaging, and neurite orientation dispersion and density imaging. Am. J. Neuroradiol. 40, 1642–1648. https://doi.org/10.3174/ajnr.A6209.
Jeurissen, B., Tournier, J.D., Dhollander, T., Connelly, A., Sijbers, J., 2014. Multi-tissue constrained spherical deconvolution for improved analysis of multi-shell diffusion MRI data. Neuroimage 103, 411–426. https://doi.org/10.1016/j.neuroimage.2014.07.061.
Kellner, E., Dhital, B., Kiselev, V.G., Reisert, M., Kiselev, V.G., Reisert, M., Kiselev, V.G., Reisert, M., 2016. Gibbs-Ringing Artifact Removal Based on Local Subvoxel-shifts. Magn. Reson. Med. 76, 1574–1581. https://doi.org/10.1002/mrm.26054.
Kelm, N.D., West, K.L., Carson, R.P., Gochberg, D.F., Ess, K.C., Does, M.D., 2016. Evaluation of diffusion kurtosis imaging in ex vivo hypomyelinated mouse brains. Neuroimage 124, 612–626. https://doi.org/10.1016/j.neuroimage.2015.09.028.
Kitley, J., Waters, P., Woodhall, M., Leite, M.I., Murchison, A., George, J., Küker, W., Chandratre, S., Vincent, A., Palace, J., 2014. Neuromyelitis optica spectrum disorders with aquaporin-4 and myelin-oligodendrocyte glycoprotein antibodies a comparative study. JAMA Neurol. 71, 276–283. https://doi.org/10.1001/jamaneurol.2013.5857.
Klistorner, A., Sriram, P., Vootakuru, N., Wang, C., Barnett, M.H., Garrick, R., Parratt, J., Levin, N., Raz, N., Van Der Walt, A., Masters, L., Graham, S.L., Yiannikas, C., 2014. Axonal loss of retinal neurons in multiple sclerosis associated with optic radiation lesions. Neurology 82, 2165–2172. https://doi.org/10.1212/WNL.0000000000000522.
Klistorner, A., Wang, C., Fofanova, V., Barnett, M.H., Yiannikas, C., Parratt, J., You, Y., Graham, S.L., 2016. Diffusivity in multiple sclerosis lesions: At the cutting edge? NeuroImage Clin. 12, 219–226. https://doi.org/10.1016/j.nicl.2016.07.003.
Kolasinski, J., Stagg, C.J., Chance, S.A., Deluca, G.C., Esiri, M.M., Chang, E.H., Palace, J. A., McNab, J.A., Jenkinson, M., Miller, K.L., Johansen-Berg, H., 2012. A combined post-mortem magnetic resonance imaging and quantitative histological study of multiple sclerosis pathology. Brain 135, 2938–2951. https://doi.org/10.1093/brain/aws242.
Lebel, C., Deoni, S., 2018. The development of brain white matter microstructure. Neuroimage 182, 207–218. https://doi.org/10.1016/j.neuroimage.2017.12.097.
Longoni, G., Brown, R.A., Momayyezsiahkal, P., Elliott, C., Narayanan, S., Bar-or, A., Ann Marrie, R., Ann Yeh, E., Filippi, M., Banwell, B., Arnold, D.L., Brown, Ã.R.A., Momayyezsiahkal, Ã.P., Elliott, C., Narayanan, S., Bar-or, A., Marrie, R.A., Yeh, E.A., Filippi, M., Banwell, B., Arnold, D.L., Pediatric, C., 2017. White matter changes in paediatric multiple sclerosis and monophasic demyelinating disorders. Brain 140, 1300–1315. https://doi.org/10.1093/brain/awx041.
Mito, R., Dhollander, T., Raffelt, D., Xia, Y., Salvado, O., Brodtmann, A., Rowe, C., Villemagne, V., Connelly, A., 2018a. Investigating microstructural heterogeneity of white matter hyperintensities in Alzheimer's disease using single-shell 3-tissue constrained spherical deconvolution. Proc. Jt. Annu. Meet, ISMRM-ESMRMB, Paris, Fr, p. 135.
Mito, R., Raffelt, D., Dhollander, T., Vaughan, D.N., Tournier, J.D., Salvado, O., Brodtmann, A., Rowe, C.C., Villemagne, V.L., Connelly, A., 2018b. Fibre-specific white matter reductions in Alzheimer's disease and mild cognitive impairment. Brain 141, 888–902. https://doi.org/10.1093/brain/awx355.
Mori, S., Oishi, K., Jiang, H., Jiang, L., Li, X., Akhter, K., Hua, K., Faria, A.V., Mahmood, A., Woods, R., Toga, A.W., Pike, G.B., Neto, P.R., Evans, A., Zhang, J., Huang, H., Miller, M.I., van Zijl, P., Mazziotta, J., 2008. Stereotaxic white matter atlas based on diffusion tensor imaging in an ICBM template. Neuroimage 40, 570–582. https://doi.org/10.1016/j.neuroimage.2007.12.035.
Muthuraman, M., Fleischer, V., Kroth, J., Ciolac, D., Radetz, A., Koirala, N., Gonzalez-Escamilla, G., Wiendl, H., Meuth, S.G., Zipp, F., Groppa, S., 2020. Covarying patterns of white matter lesions and cortical atrophy predict progression in early MS. Neurol. Neuroimmunol. neuroinflammation 7, 1–11. https://doi.org/10.1212/NXI.0000000000000681.
Ngamsombat, C., Tian, Q., Fan, Q., Russo, A., Machado, N., Polackal, M., George, I.C., Witzel, T., Klawiter, E.C., Huang, S.Y., 2020. Axonal damage in the optic radiation assessed by white matter tract integrity metrics is associated with retinal thinning in multiple sclerosis. NeuroImage Clin. 27, 102293 https://doi.org/10.1016/j.nicl.2020.102293.
Nichols, T.E., Holmes, A.P., 2002. Nonparametric permutation tests for functional neuroimaging: a primer with examples. Hum. Brain Mapp. 15 (1), 1–25.
O'Brien, R.M., 2007. A caution regarding rules of thumb for variance inflation factors. Int. J. Methodol. 41, 673–690. https://doi.org/10.1007/s11135-006-9018-6.
Pagani, E., Filippi, M., Rocca, M.A., Horsfield, M.A., 2005. A method for obtaining tract-specific diffusion tensor MRI measurements in the presence of disease: Application to patients with clinically isolated syndromes suggestive of multiple sclerosis. Neuroimage 26, 258–265. https://doi.org/10.1016/j.neuroimage.2005.01.008.
Pannek, K., Fripp, J., George, J.M., Fiori, S., Colditz, P.B., Boyd, R.N., Rose, S.E., 2018. Fixel-based analysis reveals alterations is brain microstructure and macrostructure of preterm-born infants at term equivalent age. NeuroImage Clin. 18, 51–59. https://doi.org/10.1016/j.nicl.2018.01.003.
Peterson, J.W., Bö, L., Mörk, S., Chang, A., Trapp, B.D., 2001. Transected neurites, apoptotic neurons, and reduced inflammation in cortical multiple sclerosis lesions. Ann. Neurol. 50, 389–400. https://doi.org/10.1002/ana.1123.
Pierpaoli, C., Basser, P.J., 1996. Toward a quantitative assessment of diffusion anisotropy. Magn Reson Med 36 (6), 893–906.
Popescu, V., Klaver, R., Voorn, P., Galis-De Graaf, Y., Knol, D.L., Twisk, J.W.R., Versteeg, A., Schenk, G.J., Van Der Valk, P., Barkhof, F., De Vries, H.E., Vrenken, H., Geurts, J.J.G., 2015. What drives MRI-measured cortical atrophy in multiple sclerosis? Mult. Scler. 21, 1280–1290. https://doi.org/10.1177/1352458514562440.
Raffelt, D., Tournier, J.D., Fripp, J., Crozier, S., Connelly, A., Salvado, O., 2011. Symmetric diffeomorphic registration of fibre orientation distributions. Neuroimage 56, 1171–1180. https://doi.org/10.1016/j.neuroimage.2011.02.014.
Raffelt, D., Tournier, J.D., Rose, S., Ridgway, G.R., Henderson, R., Crozier, S., Salvado, O., Connelly, A., 2012. Apparent Fibre Density: A novel measure for the analysis of diffusion-weighted magnetic resonance images. Neuroimage 59, 3976–3994. https://doi.org/10.1016/j.neuroimage.2011.10.045.
Raffelt, D.A., Smith, R.E., Ridgway, G.R., Tournier, J.D., Vaughan, D.N., Rose, S., Henderson, R., Connelly, A., 2015. Connectivity-based fixel enhancement: Whole-brain statistical analysis of diffusion MRI measures in the presence of crossing fibres. Neuroimage 117, 40–55. https://doi.org/10.1016/j.neuroimage.2015.05.039.
Raffelt, D.A., Tournier, J.D., Smith, R.E., Vaughan, D.N., Jackson, G., Ridgway, G.R., Connelly, A., 2017. Investigating white matter fibre density and morphology using fixel-based analysis. Neuroimage 144, 58–73. https://doi.org/10.1016/j.neuroimage.2016.09.029.
Rocca, M.A., Absinta, M., Amato, M.P., Moiola, L., Ghezzi, A., Veggiotti, P., Capra, R., Portaccio, E., Fiorino, A., Pippolo, L., Pera, M.C., Horsfield, M.A., Falini, A., Comi, G., Filippi, M., 2014a. Posterior brain damage and cognitive impairmen. Neurology 82, 1314–1321. https://doi.org/10.1212/WNL.0000000000000309.
Rocca, M.A., Valsasina, P., Absinta, M., Moiola, L., Ghezzi, A., Veggiotti, P., Amato, M.P., Horsfield, M.A., Falini, A., Comi, G., Filippi, M., 2014b. Intranetwork and internetwork functional connectivity abnormalities in pediatric multiple sclerosis. Hum. Brain Mapp. 35, 4180–4192. https://doi.org/10.1002/hbm.22469.
Sailer, M., Fischl, B., Salat, D., Tempelmann, C., Schönfeld, M.A., Busa, E., Bodammer, N., Heinze, H.J., Dale, A., 2003. Focal thinning of the cerebral cortex in multiple sclerosis. Brain 126, 1734–1744. https://doi.org/10.1093/brain/awg175.
Santis, S.D., Granberg, T., Ouellette, R., Treaba, C.A., Herranz, E., Fan, Q., Mainero, C., Toschi, N., De Santis, S., Granberg, T., Ouellette, R., Treaba, C.A., Herranz, E., Fan, Q., Mainero, C., Toschi, N., 2019. Evidence of early microstructural white matter abnormalities in multiple sclerosis from multi-shell diffusion MRI. NeuroImage Clin. 22, 101699 https://doi.org/10.1016/j.nicl.2019.101699.
Smith, R.E., Dimond, D., Vaughan, D., Parker, D., Dhollander, T., Jackson, G., Connelly, A., 2019. Intrinsic non-stationarity correction for Fixel-Based Analysis. Organization for Human Brain Mapping, in, p. M789.
Smith, R.E., Tournier, J.D., Calamante, F., Connelly, A., 2013. SIFT: Spherical-deconvolution informed filtering of tractograms. Neuroimage 67, 298–312. https://doi.org/10.1016/j.neuroimage.2012.11.049.
Smith, S.M., Jenkinson, M., Johansen-Berg, H., Rueckert, D., Nichols, T.E., Mackay, C.E., Watkins, K.E., Ciccarelli, O., Cader, M.Z., Matthews, P.M., Behrens, T.E.J., 2006.

Tract-based spatial statistics: voxelwise analysis of multi-subject diffusion data. Neuroimage 31, 1487–1505. https://doi.org/10.1016/j.neuroimage.2006.02.024.
Smith, S.M., Nichols, T.E., 2009. Threshold-free cluster enhancement: addressing problems of smoothing, threshold dependence and localisation in cluster inference. Neuroimage 44, 83–98. https://doi.org/10.1016/j.neuroimage.2008.03.061.
Song, H., Zhou, H., Yang, M., Xu, Q., Sun, M., Wei, S., 2019. Clinical characteristics and outcomes of myelin oligodendrocyte glycoprotein antibody-seropositive optic neuritis in varying age groups: A cohort study in China. J. Neurol. Sci. 400, 83–89. https://doi.org/10.1016/j.jns.2019.03.014.
Steenwijk, M.D., Geurts, J.J.G., Daams, M., Tijms, B.M., Wink, A.M., Balk, L.J., Tewarie, P.K., Uitdehaag, B.M.J., Barkhof, F., Vrenken, H., Pouwels, P.J.W., 2016. Cortical atrophy patterns in multiple sclerosis are non-random and clinically relevant. Brain 139, 115–126. https://doi.org/10.1093/brain/awv337.
Storelli, L., Pagani, E., Preziosa, P., Filippi, M., Rocca, M.A., 2021. Measurement of white matter fiber-bundle cross-section in multiple sclerosis using diffusion-weighted imaging. Mult. Scler. J. 27 (6), 818–826.
Tamnes, C.K., Herting, M.M., Goddings, A.L., Meuwese, R., Blakemore, S.J., Dahl, R.E., Güroğlu, B., Raznahan, A., Sowell, E.R., Crone, E.A., Mills, K.L., 2017. Development of the cerebral cortex across adolescence: A multisample study of inter-related longitudinal changes in cortical volume, surface area, and thickness. J. Neurosci. 37, 3402–3412. https://doi.org/10.1523/JNEUROSCI.3302-16.2017.
Thompson, A.J., Banwell, B.L., Barkhof, F., Carroll, W.M., Coetzee, T., Comi, G., Correale, J., Fazekas, F., Filippi, M., Freedman, M.S., Fujihara, K., Galetta, S.L., Hartung, H.P., Kappos, L., Lublin, F.D., Marrie, R.A., Miller, A.E., Miller, D.H., Montalban, X., Mowry, E.M., Sorensen, P.S., Tintoré, M., Traboulsee, A.L., Trojano, M., Uitdehaag, B.M.J., Vukusic, S., Waubant, E., Weinshenker, B.G., Reingold, S.C., Cohen, J.A., 2018. Diagnosis of multiple sclerosis: 2017 revisions of the McDonald criteria. Lancet Neurol. 17, 162–173. https://doi.org/10.1016/S1474-4422(17)30470-2.
Till, C., Deotto, A., Tipu, V., Sled, J.G., Bethune, A., Narayanan, S., Arnold, D.L., Banwell, B.L., 2011. White matter integrity and math performance in pediatric multiple sclerosis: A diffusion tensor imaging study. NeuroReport 22, 1005–1009. https://doi.org/10.1097/WNR.0b013e32834dc301.
Tillman, J., Leach, J., Pirko, I., 2012. Non-lesional white matter changes in pediatric multiple sclerosis and monophasic demyelinating disorders. Mult. Scler. J. 18, 1754–1759. https://doi.org/10.1093/brain/awx041.
Tournier, J.-D., Calamante, F., Gadian, D.G., Connelly, A., 2004. Direct estimation of the fiber orientation density function from diffusion-weighted MRI data using spherical deconvolution. Neuroimage 23, 1176–1185. https://doi.org/10.1016/j.neuroimage.2004.07.037.
Tournier, J.-D.-D., Smith, R.E., Raffelt, D., Tabbara, R., Dhollander, T., Pietsch, M., Christiaens, D., Jeurissen, B., Yeh, C.-H.-H., Connelly, A., 2019. MRtrix3: A fast, flexible and open software framework for medical image processing and visualisation. Neuroimage 202, 116137. https://doi.org/10.1101/551739.
Tournier, J.D., Calamante, F., Connelly, A., 2010. Improved probabilistic streamlines tractography by 2nd order integration over fibre orientation distributions, in: Proceedings of the 18th Annual Meeting of ISMRM. Stockholm, Sweden. p. 1670.
Tsagkas, C., Chakravarty, M.M., Gaetano, L., Naegelin, Y., Amann, M., Parmar, K., Papadopoulou, A., Wuerfel, J., Kappos, L., Sprenger, T., Magon, S., Wuerfel, J., Kappos, L., 2020. Longitudinal patterns of cortical thinning in multiple sclerosis. Hum. Brain Mapp. 41, 2198–2215. https://doi.org/10.1002/hbm.24940.
Tuch, D.S., Reese, T.G., Wiegell, M.R., Wedeen, V.J., 2003. Diffusion MRI of complex neural architecture. Neuron 40, 885–895.
Veraart, J., Fieremans, E., Jelescu, I.O., Knoll, F., Novikov, D.S., 2016a. Gibbs ringing in diffusion MRI. Magn. Reson. Med. 76, 301–314. https://doi.org/10.1002/mrm.25866.
Veraart, J., Novikov, D.S., Christiaens, D., Ades-aron, B., Sijbers, J., Fieremans, E., 2016b. Denoising of diffusion MRI using random matrix theory. Neuroimage 142, 394–406. https://doi.org/10.1016/j.neuroimage.2016.08.016.
Veraart, J., Sijbers, J., Sunaert, S., Leemans, A., Jeurissen, B., 2013. Weighted linear least squares estimation of diffusion MRI parameters: Strengths, limitations, and pitfalls. Neuroimage 81, 335–346. https://doi.org/10.1016/j.neuroimage.2013.05.028.
Vijayakumar, N., Allen, N.B., Youssef, G., Dennison, M., Yücel, M., Simmons, J.G., Whittle, S., 2016. Brain development during adolescence: A mixed-longitudinal investigation of cortical thickness, surface area, and volume. Hum. Brain Mapp. 37, 2027–2038. https://doi.org/10.1002/hbm.23154.
Vishwas, M.S., Chitnis, T., Pienaar, R., Healy, B.C., Grant, P.E., 2010. Tract-based analysis of callosal, projection, and association pathways in pediatric patients with multiple sclerosis: A preliminary study. Am. J. Neuroradiol. 31, 121–128. https://doi.org/10.3174/ajnr.A1776.
Vishwas, M.S., Healy, B.C., Pienaar, R., Gorman, M.P., Grant, P.E., Chitnis, T., 2013. Diffusion tensor analysis of pediatric multiple sclerosis and clinically isolated syndromes. Am. J. Neuroradiol. 34, 417–423. https://doi.org/10.3174/ajnr.A3216.
Vos, S.B., Jones, D.K., Jeurissen, B., Viergever, M., a, Leemans, A.,, 2012. The influence of complex white matter architecture on the mean diffusivity in diffusion tensor MRI of the human brain. Neuroimage 59, 2208–2216. https://doi.org/10.1016/j.neuroimage.2011.09.086.
Waldman, A.T., Sollee, J.R., Datta, R., Lavery, A.M., Liu, G., Aleman, T.S., Banwell, B.L., Gaetz, W.C., Lavery, A.M., Gaetz, W.C., 2020. Structural correlates of atypical visual and motor cortical oscillations in pediatric-onset multiple sclerosis. Hum. Brain Mapp. 41, 4299–4313. https://doi.org/10.1002/hbm.25126.
Wedeen, V.J., Hagmann, P., Tseng, W.-Y.-I., Reese, T.G., Weisskoff, R.M., 2005. Mapping complex tissue architecture with diffusion spectrum magnetic resonance imaging. Magn Reson Med 54, 1377–1386. https://doi.org/10.1002/mrm.20642.
Wierenga, L.M., Langen, M., Oranje, B., Durston, S., 2014. Unique developmental trajectories of cortical thickness and surface area. Neuroimage 87, 120–126. https://doi.org/10.1016/j.neuroimage.2013.11.010.
Wilbur, C., Reginald, Y.A., Longoni, G., Grover, S.A., Wong, A.M., Mabbott, D.J., Arnold, D.L., Marrie, R.A., Bar-Or, A., Banwell, B., Costello, F., Yeh, E.A., 2019. Early neuroaxonal injury is seen in the acute phase of pediatric optic neuritis. Mult. Scler. Relat. Disord. 36, 101387 https://doi.org/10.1016/j.msard.2019.101387.
Yotter, R.A., Nenadic, I., Ziegler, G., Thompson, P.M., Gaser, C., 2011. Local cortical surface complexity maps from spherical harmonic reconstructions. Neuroimage 56, 961–973. https://doi.org/10.1016/j.neuroimage.2011.02.007.
Zhang, H., Schneider, T., Wheeler-Kingshott, C.A., Alexander, D.C., 2012. NODDI: Practical in vivo neurite orientation dispersion and density imaging of the human brain. Neuroimage 61, 1000–1016. https://doi.org/10.1016/j.neuroimage.2012.03.072.
Ziegler, G., Ridgway, G.R., Blakemore, S.J., Ashburner, J., Penny, W., Ridgway, G.R., Blakemore, S.J., Ashburner, J., 2017. Multivariate dynamical modelling of structural change during development. Neuroimage 147, 746–762. https://doi.org/10.1016/j.neuroimage.2016.12.017.